# Magnetic Solitons in the 1-D Antiferromagnetic Chains of $Li_2Mn_{0.98}Fe_{0.02}F_5$ and $Na_2Mn_{0.98}Fe_{0.02}F_5$

Ch. Frommen*, M. Mangold, and J. Pebler

Fachbereich Chemie und Wiss. Zentrum für Materialwissenschaften der Philipps-Universität, Hans-Meerwein-Str., D-35043 Marburg

Z. Naturforsch. **51a**, 939–949 (1996); received February 1, 1996

*Prof. Dr. Kurt Dehnicke zum 65. Geburtstag gewidmet*

Measurements of the $^{57}$Fe Mössbauer effect and magnetic susceptibility have been performed on $^{57}$Fe-doped quasi-1-d antiferromagnetic chains of $Li_2MnF_5$ and $Na_2MnF_5$ as a function of temperature. The Mössbauer spectra, fitted by the Blume-Tjon model, show definite relaxation effects near the Néel temperature, which are attributed to short-range order with temperature-dependent relaxation times. The soliton model of non-linear excitations was applied. Experimental data confirm the predicted exponential temperature dependence of the thermal excitation of moving domain walls. From the activation energies $E_A^2/k^2$ as a function of 1-d exchange energies $J/k$ the local anisotropy energy $D/k$ of $-3.7(2)$ K was derived on the basis of sine-Gordon theory. This result is in fair agreement with $-3.5(1)$ K previously derived from magnetic susceptibility measurements. In the light of our results there is some evidence that at low bridging angle $\beta \approx 102(5)^\circ$ a phase-transition from antiferromagnetic to ferromagnetic ordering occurs.

*Key words:* Magnetization, Exchange and Anisotropy Energy, Relaxation, Solitons.

## Introduction

Extended spin fluctuations can be observed over a wide range of temperature in one dimensional magnetic lattices, and this is one of the interesting points in the study of such a system [1–9]. In these compounds, linear physics involving magnons or spin waves appears to be insufficient to describe their physical properties, and non-linear physics becomes dominant. Non-linear excitation, as a soliton, is the magnetic domain wall which is the transition region between two different but energetically degenerate ground states in magnetic systems with easy-axis anisotropy. In a ferromagnet, a $\pi$-soliton mediates a spin up and spin down region. Similar $\pi$-solitons separate degenerate ground state configurations of the antiferromagnetic chain, which are obtained by a simultaneous rotation of the spins of the two sublattices over an angle $\pi$. One uses the term soliton for the large amplitude solutions of a non-linear differential equation, e.g. the sine-Gordon equation.

The static properties of the 1-d domain walls, with wall energy $E_s$ and wall-width $N_s$, may be estimated from the corresponding Hamiltonian. Assuming that the spin $S$ is large enough to allow the approximation of the quantum-mechanical spins by classical spin vectors, the chain may be described by the hamiltonian

$$\boldsymbol{H} = \sum (2J\boldsymbol{S}_i\boldsymbol{S}_{i+1} + D(S_{iz}^2) + E(S_{i,x}^2 - S_{i,y}^2)), \qquad (1)$$

where $S$ and $S_x (= x, y, z)$ are spin operators relating to the occupied energy levels. The chain direction is along the $z$ axis. The first term represents an isotropic Heisenberg exchange interaction between two neighbouring spins on the chain. $D$ and $E$ are the axial and orthorhombic crystal field parameters. The single-ion-type anisotropy may arise from the crystal field potential. The orthorhombic term takes into account the anisotropy in the plane perpendicular to the principal axis. It can be shown that $E \ll D$ and $J > D$ for all cases of interest here in which the magnetic moments are directed along the chains. In the classical domain wall theory [10] the wall energy $E_s$ from (1) with $D \gg E$ is simply the sum of the contributions due to the exchange energy and anisotropy, yielding

$$E_s = \pi^2 J S^2 / N_s + N_s D S^2 . \qquad (2)$$

Stability requires $E_s$ to be a minimum, and after minimization with respect to $N_s$ one obtains [11]

$$E_s = 2\pi S^2 |DJ|^{1/2} \quad \text{and} \quad N_s = \pi |J/D|^{1/2} . \qquad (3)$$

* Department of Chemistry, University of Sheffield, Western Bank, Sheffield 53 7HF, U.K.

Reprint requests to Prof. Dr. J. Pebler.

0932-0784 / 96 / 0800-0939 $ 06.00 © – Verlag der Zeitschrift für Naturforschung, D-72072 Tübingen

In comparison with these results of the classical domain wall theory, solutions of the sine-Gordon equation yield [11]

$$E_s = 4S^2|DJ|^{1/2} \quad \text{and} \quad N_s = |J/D|^{1/2} \tag{4}$$

for the ferro- and antiferromagnetic chain systems. As far as the static properties of the solitons are concerned, there is no difference (except for a factor $\pi/2$) at all between the various approximations. It is remarkable that the elementary classical domain wall theory [10, 11] already yields the correct order of magnitude and functional dependence of exchange and anisotropy energy.

Solitons in magnetic chains are moving domain walls. Their structure is determined by the competition between the exchange energy $J$ (which favours a broad wall) and the anisotropy energy $D$ (which favours a narrow wall). In highly anisotropic chain compounds, the soliton width $N_s$ decreases to zero. Under the assumption that the "narrow" solitons neither interact with other solitons nor with the lattice, they can be described as an ideal soliton gas [11]. These free solitons have the interesting feature that their energy is preserved when they are moving along the chains. In the free gas approximation the soliton density $n_s$ increases exponentially with temperature: $n_s \propto \exp(-E_s/kT)$ [12]. A passing $\pi$-wall flips the electron spin. The flipping rate $G_\omega$ is proportional to the product $n_s v_s$ of wall density and average wall velocity $v_s$, so that

$$G_\omega = \exp(-E_s/kT), \tag{5}$$

where $E_s$ is the excitation energy for solitons. The average time between two flips amounts to $G_\omega^{-1}$.

The dynamic behaviour of the solitons determines the spin correlation function [12]. These solitons may be conveniently studied in real quasi-1-d ionic compounds, e.g. in $^{57}$Fe doped fluoromanganates(III) with easy-axis anisotropy in which the magnetic moments are arranged in widely separated chains such that the ratio of interchain to intrachain exchange interaction $J'/J$ is very small [13–16]. A domain wall that passes the Mössbauer ion flips the hyperfine field $H_{hf}$, and the flip rate may become low enough to fall within the Mössbauer frequency window. With the aid of Mössbauer spectroscopy one probes the autocorrelation function,

$$\langle \boldsymbol{H}_{hf}(t)\,\boldsymbol{H}_{hf}(0)\rangle \propto \langle S^z(t)\,S^z(0)\rangle = \langle S_z^2\rangle \exp(-G_\omega t), \tag{6}$$

of the electronic spins on the magnetic chain [12].

In previous papers we have shown that for $^{57}$Fe doped fluoromanganates (III) like $Rb_2Mn_{0.99}Fe_{0.01}F_5(H_2O)$ [13] and $(NH_4)_2Mn_{0.98}Fe_{0.02}F_5$ [17] with strong local anisotropy, the frequency range of $G_\omega$ covers many orders of magnitude, typically from $10^5$ up to $10^{11}$ Hz. The activation energies $E_A$ for $Rb_2Mn_{0.99}Fe_{0.01}F_5(H_2O)$ and $(NH_4)_2Mn_{0.98}Fe_{0.02}F_5$ derived from Mössbauer relaxation spectra decrease from 234 K to 166 K corresponding to a change of the Mn-F-Mn bridging angles from 175.4° to 143.4° and a change of the energy from $J/k = -20.0$ K to $J/k = -10.6$ K [13–17].

In the following study we present experimental results obtained by Mössbauer spectroscopy for the quasi-1-d magnetic chains of $Li_2Mn_{0.98}Fe_{0.02}F_5$ and $Na_2Mn_{0.98}Fe_{0.02}F_5$. We discuss in some detail the influence of a small bridging angle $\beta$(Mn-F-Mn) ($\beta = 121.5°$ for $Li_2MnF_5$; $\beta = 132.5°$ for $Na_2MnF_5$ [18]) on the dynamic and static properties of the nonlinear excitations extracted from a series of Fe(III) Mössbauer spectra and measurements of the magnetic powder susceptibilities. We pay attention to the relationship between the soliton activation energy and the 1-d exchange energy proposed by the soliton theory. In doing so, our aim is to test how far the magnetic anisotropy can be extracted from dynamic properties of powder samples with the aid of Mössbauer spectroscopy.

## Experimental

The powder sample of $Li_2MnF_5$ was prepared by the solid state reaction of a stoichiometric mixture of LiF and $MnF_3$ in a sealed platinum tube at 650 °C [19]. $Na_2MnF_5$ was prepared in an aqueous solution of 2 N HF using $Mn(OOCCH_3)_3 \cdot 2H_2O$ and $Na_2CO_3$ [20]. The $^{57}$Fe samples of $Li_2Mn_{0.98}Fe_{0.02}F_5$ and $Na_2Mn_{0.98}Fe_{0.02}F_5$ for Mössbauer study were prepared in a similar way, using $^{57}FeF_3$ in the case of solid state reaction and $^{57}$Fe metal for the reaction carried out in aqueous HF. The $^{57}$Fe was dissolved and oxidized in 40% HF using small amounts of 30% $H_2O_2$, thus yielding $^{57}FeF_3$(aq). An excess of $H_2O_2$ was removed by heating the solution in a platinum crucible and refilling with 40% HF.

Magnetic data were obtained from 1.8 to 330 K by using a SQUID magnetometer in a magnetic field from −55 up to 55 kG [21]. Mössbauer measurements

Table 1. Space groups SG, bridge angle $\beta$(Mn-F-Mn), metal–metal distances M–M and M–M′ within and between the chains, respectively, and axial and equatorial M–F distances for the compounds listed below.

| Compound | SG | $\beta$ [°] | M–M [Å] | M′–M [Å] | $M_{eq}$ [Å] | $M_{ax}$ [Å] | $M_{ax}/M_{eq}$ |
|---|---|---|---|---|---|---|---|
| $Li_2MnF_5$ [19] | C2/c | 121.5 | 3.700 | 4.948 | 1.847 | 2.123 | 1.149 |
| $Na_2MnF_5$ [19, 20] | $P2_1/c$ | 132.5 | 3.860 | 5.236 | 1.849 | 2.109 | 1.141 |
| $(NH_4)_2MnF_5$ [19, 22] | Pnma | 143.4 | 3.970 | 6.219 | 1.853 | 2.091 | 1.128 |
| $Rb_2MnF_5(H_2O)$ [18, 19, 23] | Cmcm | 175.4 | 4.170 | 6.235 | 1.848 | 2.089 | 1.130 |

were performed from 1.8 to 300 K by using standard equipment described in [13] and a 20 mCi $^{57}$Co(Rh) source.

## Crystallographic Characterization

The structures of $Li_2MnF_5$ and $Na_2MnF_5$ were first solved by Massa et al. [19, 20]. Both compounds show monoclinic symmetry (see Table 1): (SG. C2/*c*, $Z = 4$, $a = 10.016(1)$, $b = 4.948(1)$, $c = 7.408(1)$ Å, $\beta = 112.19(1)°$ for $Li_2MnF_5$; SG. $P2_1/c$, $Z = 4$, $a = 7.719(1)$, $b = 5.236(1)$, $c = 10.862(2)$ Å, $\beta = 108.99(1)°$ for $Na_2MnF_5$). Isolated infinite chains of trans-linked $[MnF_4F_{2/2}]^{2-}$-octahedra run along the *b* direction with a bridging angle of $\beta$(Mn-F-Mn) = 121.5(1)° and 132.5(1)°, respectively. The individual chains are separated by Li and Na ions. The mean interatomic Mn-F distances are Mn-$F_{ax}$ = 2.123(1) Å, Mn-$F_{eq}$ = 1.846(1) Å for $Li_2MnF_5$, and Mn-$F_{ax}$ = 2.109(1) Å and Mn-$F_{eq}$ = 1.849(1) Å for $Na_2MnF_5$.

All fluoromanganate(III) structures of the type $A_2MnF_5(H_2O)$ with A = Li, Na, $NH_4$, Rb show strongly elongated $[MnF_4F_{2/2}]^{2-}$ octahedra, similar to the other "strong" Jahn-Teller systems with Cr(II) or Cu(II). Due to the stabilization energy [18], the Jahn-Teller elongation always points towards the octahedral axis bearing the weakest bonds. Thus, in the trans chain compounds the weaker bridging bonds along the chain direction undergo an additional substantial weakening (Figure 1). One observes a ferrodistortive ordering of elongated octahedra. The direction of the elongation indicates the orientation of the half-occupied $d_z^2$ orbital stabilized by the elongation. Variation of the counter cation A allows a "tuning" of bridge angles (Table 1) whereas the local geometry of the $[MnF_4F_{2/2}]^{2-}$ octahedra remains almost unchanged. The small briding angles for $Li_2MnF_5$ and $Na_2MnF_5$ can be explained by the tendency of $Li^+$ and $Na^+$ to obtain a coordination number of 6 comparing with 12 for $Rb_2MnF_5(H_2O)$ [22, 23]. Thus, these chain structures seem to be a good model system for studies of the angular dependence of exchange and soliton activation energies. The molecular *z* axes (of the $D_{4h}$ molecular unit) of $Li_2MnF_5$ and $Na_2MnF_5$ are taken parallel to the 3.70 Å and 3.86 Å bond directions and thus make angles of 29.3° and 23.7° with the *b* crystallographic axes, respectively. The coordination around Mn(III) is very nearly axially symmetric (rhombic distortion is less than 0.1%). The EPR spectra of the analogous chain compound $(NH_4)_2MnF_5$ (space group Pnma, $Z = 4$) at room temperature are nearly isotropic with two small signals at the values $g_\perp = 2.002$ and $g_\parallel = 1.997$ [24]. Then, in our case for local orthorhombic symmetry, the influence of zero-field splitting on the measurable magnetic properties can be accounted for by considering (1) in the modified form

$$\boldsymbol{H} = \sum \left[ 2J\boldsymbol{S}_i S_{i+1} + D\left( S_{iz}^2 + \frac{1}{3} S(S+1) \right) \right]. \qquad (1\,b)$$

Kida and Watanabe [25] had determined the zero-field splitting $D/k$ for $(NH_4)_2MnF_5$ to $-3.31$ K.

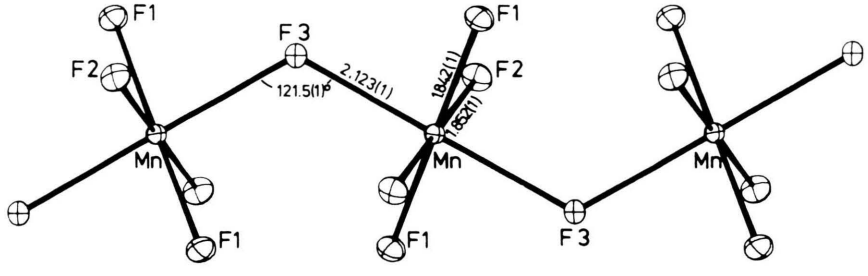


Fig. 1. Ferrodistortive ordering of elongated octahedra in $Li_2MnF_5$. Distances are in Å. Thermal ellipsoids at 50% probability level [19].

They found that the spins are parallel to the chain axis. This uniaxial spin direction was also confirmed for Fe(III)/Mn(III) ions in the case of the solid solutions $(NH_4)_2Mn_{1-x}Fe_xF_5$ and $Rb_2Mn_{1-x}Fe_xF_5(H_2O)$ for the range $x < 0.5$ [13, 26]. Since Fe(III) is $3d^5$, the single-ion anisotropy of Fe(III) will be negligible. Mn(III) is $3d^4$ and so should have strong anisotropic properties, which are transmitted via Mn-Fe exchange to the Fe atoms. The latter become polarized in the same direction as the Mn spins. We assume that a similar interaction exists in $Li_2Mn_{0.98}Fe_{0.02}F_5$ and $Na_2Mn_{0.98}Fe_{0.02}F_5$.

## Magnetic Susceptibility

Since we failed to obtain appropriate single crystals we have performed magnetic susceptibility measurements on powders of the compounds $Li_2Mn_{1-x}Fe_xF_5$ and $Na_2Mn_{1-x}Fe_xF_5$ ($x = 0$ and $x = 0.02$) with the aid of our SQUID-Magnetometer [21]. The results for the pure manganese compounds agree within experimental error with our former measurements obtained with a VSM [19].

Measurements of the magnetic powder susceptibility of $Li_2Mn_{0.98}Fe_{0.02}F_5$ and $Na_2Mn_{0.98}Fe_{0.02}F_5$ show a broad maximum in the $\chi$ versus $T$ curve at $T(\chi_{max}) = 35$ K and 50 K, respectively. They are undoubtedly due to short-range antiferromagnetic interactions within the linear chains (see Figures 2–3). Assuming $S = 2$ and $g = 2$ we have fitted Fisher's expression [27, 28] for the magnetic powder susceptibility of a chain to our data by adjusting the exchange energy $J/k$:

$$X(T) = \frac{Ng^2 \mu_B^2 S(S+1)}{3kT} \frac{(1+u)}{(1-u)}, \qquad (7)$$

where

$$u = \coth K - K^{-1} \quad \text{and} \quad K = \frac{2JS(S+1)}{kT}.$$

The best fits were obtained for $Li_2Mn_{0.98}Fe_{0.02}F_5$ and $Na_2Mn_{0.98}Fe_{0.02}F_5$ with $g = 2.0$, $J/k = -5.9(2)$ K, and $g = 2.0$, $J/k = -8.4(2)$ K, respectively (see Figures 2 and 3).

For $T > T(\chi_{max})$ the spin correlations vanish and the compounds behave like normal paramagnets with a Curie-Weiss susceptibility. From a least squares fit we have calculated the Curie-Weiss temperatures $\theta_p$ listed in Table 2.

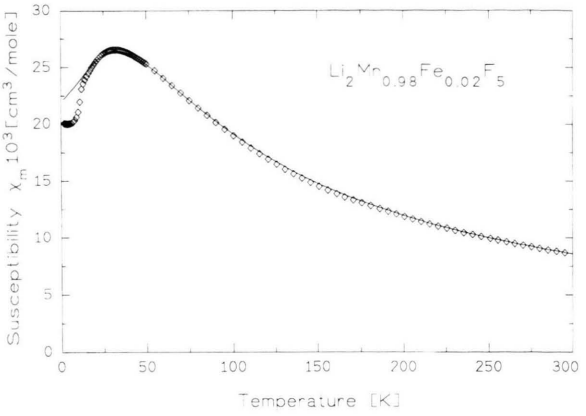


Fig. 2. Magnetic powder susceptibilities of $Li_2Mn_{0.98}Fe_{0.02}F_5$. The symbols are data points. The continous line is the solution for the classical Heisenberg linear chain, as described in the text.

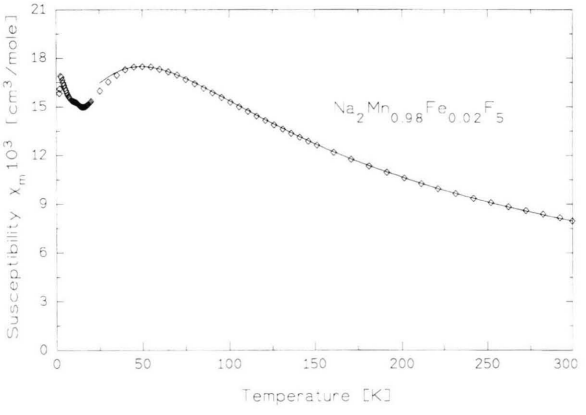


Fig. 3. Magnetic powder susceptibilities of $Na_2Mn_{0.98}Fe_{0.02}F_5$. The points are experimental, and the curve is fitted as described in the text.

Strong evidence of three dimensional long range ordering is given from the appearance of hysteresis phenomena and residual magnetization. The discrepancy between theory according to (7) and experiment below $T(\chi_{max})$ is probably due to the existence of a weakly canted rather than a strictly antiferromagnetic spin arrangement below the ordering temperatures $T_N$, leading to a divergence of susceptibilities.

From single crystal measurements on $Rb_2MnF_5(H_2O)$ [29], $K_2MnF_5(H_2O)$ [29], $enH_2MnF_5$ [30], and $(NH_4)_2MnF_5$ [17] we find that the spins are nearly antiparallel to the $z$ axis (chain direction), but they have small canted components along the $x$ axis (per-

Table 2. Calculated canting angles $\varphi$ (see (8)), Curie-Weiss temperatures $\theta_p$, intra-chain exchange energies $J$, Néel temperatures $T_N$, and inter-chain energies $J'$, and anisotropy constants $D$ for the compounds listed.

| Compound | $\varphi$ [°] | $\theta_p$ [K] | $J/k$ [K] | $T_N$ [K] | $\lvert J'/k \rvert$ [K] | $D/k$ [K] |
|---|---|---|---|---|---|---|
| $Li_2MnF_5$ | 7.3 | −66(5) | −5.9(2) | 4.2(5) | 0.046 | – |
| $Li_2R$ | | −68(5) | −5.9(2) | 4.4(5) | 0.052 | – |
| $Na_2MnF_5$ | 3.0 | −91(5) | −8.4(2) | 6.0(5) | 0.063 | – |
| $Na_2R$ | | −90(5) | −8.5(2) | 6.2(5) | 0.061 | – |
| $(NH_4)_2MnF_5$ | 1.6 | −153(5) | −10.6(2) | 8.5(5) | 0.095 | −3.5(3) [19] |
| | | | | | | −3.3 [25] |
| $enH_2MnF_5$ | 0.7 | −214(5) | −13.6(2) | 14.5(5) | 0.22 | −3.5(3) [30] |
| $Rb_2MnF_5(H_2O)$ | 0.1 | −428(5) | −20.0(2) | 23.0(7) | 0.353 | −3.5(3) [13] |

R =: $Mn_{0.98}Fe_{0.02}F_5$.

pendicular to the chain direction) in the ordered state which produce a weak ferromagnetism observed in the compounds above. The chain direction is denoted as $z$ axis independent of the crystallographic orientation. The canting angle $\varphi$ is caused by the local anisotropy ($D/k = -3.5(2)$ K) producing a different preferential direction for the moments which are on different sublattices. This mechanism occurs when the local arrangement of the atoms around the sites of the magnetic ions are tilted with respect to each other. As long like as we treat the problem an isolated chain [25], the canting angle $\varphi$ of the spins is obtained as

$$\tan\varphi = \frac{D\left(1-\frac{1}{2S}\right)\sin(\delta)}{2zJ + D\left(1-\frac{1}{2S}\right)\cos(\delta)}, \qquad (8)$$

where $z$ denotes the number of nearest neighbouring spins. The direction of local anisotropy for each sublattice is assumed to make an angle $\delta = (180° - \beta)/2$ with the positive or negative $z$ axis. If the preferred direction due to the anisotropy is the same for both sublattices ($\delta = 0$), the canting angle $\varphi$ is evidently equal to zero. An increase of $\delta$ also increases the canting angle. If, on the other hand, the exchange interaction $J$ is zero it is easily seen that $\varphi = \delta$. When the appropriate values of the parameters are substituted, the canting angles are obtained as given in Table 2. We calculate from (8) for $Li_2MnF_5$ and $Na_2MnF_5$ the canting angles of 7.3(5)° and 3.0(5)°, respectively. Thus, the linear chains as a whole give fractional weak ferromagnetic moments of about 0.5 and 0.2 $\mu_B$ per ion [29] which are orientated perpendicular to the chain direction for $T < T_N$, as observed in our single crystal measurements. As we have shown in previous work, this weak ferromagnetic component is qualitatively visible in a weak magnetic field [26]. Therefore,

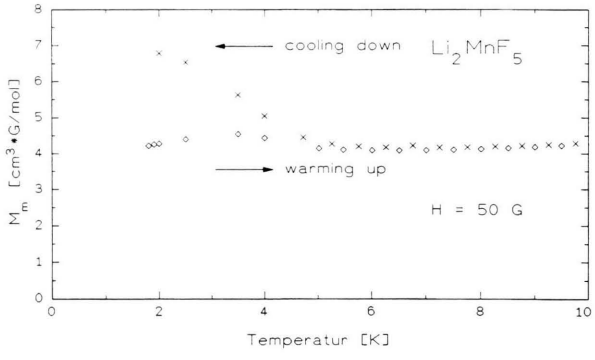


Fig. 4. Magnetization in a small magnetic field of 50 G after zero-field cooling for $Li_2Mn_{0.98}Fe_{0.02}F_5$.

in order to get informations about spin canting and the ordering temperature $T_N$ we measured for $Li_2MnF_5$ and $Na_2MnF_5$, after zero-field cooling, the magnetization in an external magnetic field of 50 G within the temperature range between 1.8 and 25 K. After this procedure we cooled down in the same field. The different branches of magnetization for $Li_2MnF_5$ and $Na_2MnF_5$ diverge at 4.2 K and 6 K, respectively, typically for weak ferromagnetism in the ordered state (Fig. 4 and Table 2). We define these temperatures as the Néel temperatures for our compounds, as done in former experiments [29–32] where the temperature of divergence of magnetization coincided with $T_N$ derived from single crystal studies of magnetic susceptibilities. Most recently, these 3-d ordering temperatures for $Rb_2MnF_5(H_2O)$ and $(NH_4)_2MnF_5$ derived in a weak magnetic field were confirmed by inelastic neutron diffraction experiments [33, 34].

In quasi 1-d magnets the temperature $T_N$ at which the transition to a 3-d ordered state occurs is proportional to the intrachain correlation length $\zeta(T)$. In a system of weakly coupled chains, the ordering

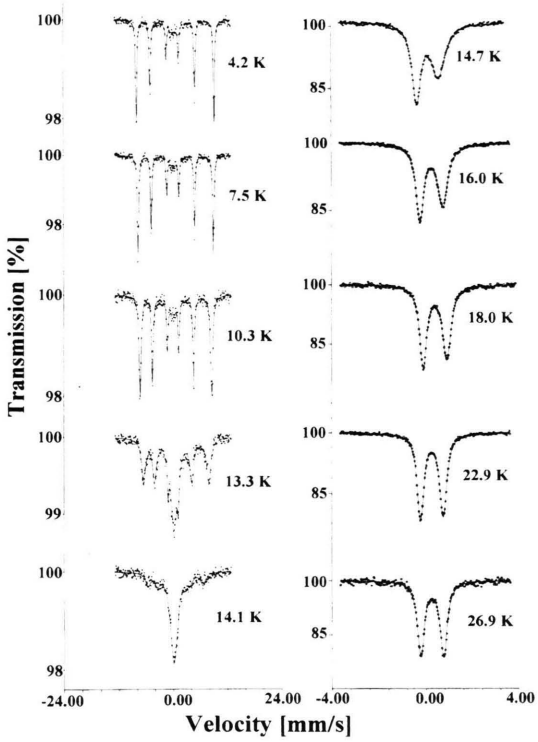


Fig. 5. Temperature dependence of the Mössbauer spectra for a powder sample of $Li_2Mn_{0.98}Fe_{0.02}F_5$. The continous line represents a least-squares fit to the applied relaxation model. Please, note the different velocity scales in the left and right hand column.

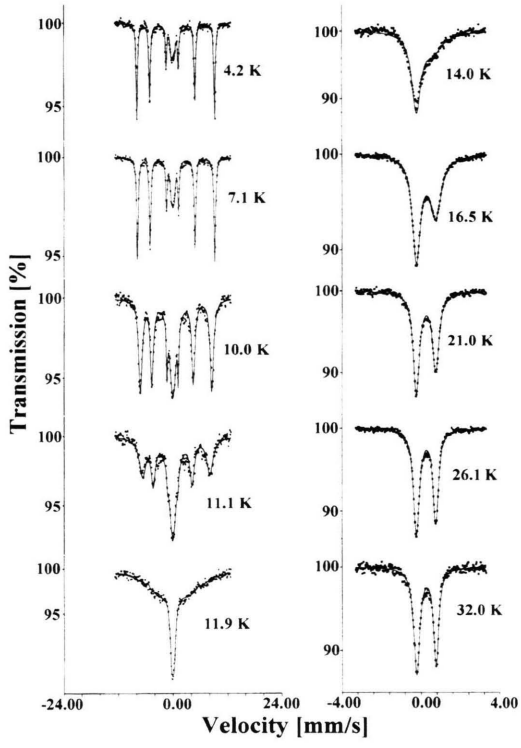


Fig. 6. Temperature dependence of the Mössbauer spectra for a powder sample of $Na_2Mn_{0.98}Fe_{0.02}F_5$. Please, note the different velocity scales in the left and right hand column.

temperature can be considered as the temperature at which the thermal energy equals the interaction energy between correlated chain segments: $kT_N/|J| = \zeta(T_N)RS(S+1)$, where $\zeta(T_N)$ is the correlation length within the chain and $R = J'/J$ is the ratio of inter- to intra-chain exchange. For a Heisenberg chain [12], $\zeta(T) = 2|J|S(S+1)/kT$ so that $kT_N/|J| = S(S+1)\ (2R)^{1/2}$. Using our results for $Li_2Mn_{0.98}Fe_{0.02}F_5$ and $Na_2Mn_{0.98}Fe_{0.02}F_5$ with $J/k = -6.2(2)$ K, $T_N = 4.0(2)$ K, and $J/k = -8.2(2)$ K, $T_N = 6(2)$ K, respectively we obtain $R = J'/J = 6.7 \cdot 10^{-3}$, $J'/k = -0.04$ K, and $R = J'/J = 7.6 \cdot 10^{-3}$, $J'/k = -0.06$, respectively. Since $\zeta$ will become appreciable for $kT < |J|S(S+1)$, the region in which to study 1-d excitations is approximately defined by $T_N < T < |J|S(S+1)/k \approx T(\chi_{max})$ equal to 64 K and 69 K, respectively. Comparing the results for $Li_2Mn_{0.98}Fe_{0.02}F_5$ and $Na_2Mn_{0.98}Fe_{0.02}F_5$ with those measured on the pure compounds, the results are much the same.

## $^{57}$Fe Mössbauer Effect

The temperature dependence of the Mössbauer spectra for powder samples of $Li_2Mn_{0.98}Fe_{0.02}F_5$ and $Na_2Mn_{0.98}Fe_{0.02}F_5$ are shown in Fig. 5 and Fig. 6, respectively. The spectra were analyzed by fitting symmetric Lorentzian lines. Above 50 K the spectra were essentially the same. There is, as already discussed for $Rb_2Mn_{0.99}Fe_{0.01}F_5$ [13], $(NH_4)_2Mn_{0.98}Fe_{0.02}F_5$ [17], and $enH_2Mn_{0.98}Fe_{0.02}F_5$ [30], some slight temperature-independent asymmetry over this temperature range that we attribute to sample texture. The two lines have unequal intensities, the lower energy one being more intense. This can be explained by non-random orientation of crystallites in the absorber, since sample-crystals readily cleave in chaines parallel to the absorber planes. From the intensity difference we concluded that the lower-energy line is the $(\pm 1/2 \rightarrow \pm 1/2)$ line and that the quadrupole splittings for $Fe^{3+}$ in $Li_2MnF_5$ and $Na_2MnF_5$ are positive in agreement

with the results for $(NH_4)_2Mn_{0.98}Fe_{0.02}F_5$ [17], $Rb_2Mn_{1-x}Fe_xF_5(H_2O)$ [13], and $enH_2Mn_{0.98}Fe_{0.02}F_5$ [30]. At lower temperatures between 26 and 14 K for the Li compound and between 32 and 12 K for the Na compound, an additional temperature-dependent asymmetry of the absorption lines was observed. As the temperature was further decreased, the spectra exhibited magnetic hyperfine splitting. Between about 14 and 10 K the quadrupole doublets of the paramagnetic phases disappeared for both compounds. The transition to the magnetically split phase was accompanied by a strong broadening of the lines and the apparent coexistence of contributions from the paramagnetic and magnetically ordered phase. Below $T_N$ the line widths returned to normal. For $Li_2Mn_{0.98}Fe_{0.02}F_5$, an almost pure combined hyperfine pattern was observed. Interestingly, in the case of $Na_2Mn_{0.98}Fe_{0.02}F_5$ a contribution from the paramagnetic phase was observed even at the lowest temperatures.

As mentioned above, the coordination around $Mn^{3+}$ and $Fe^{3+}$ is very nearly axially symmetric. The site symmetry at the Mössbauer nucleus contains a four-fold rotation axis $D_{4h}$, coinciding with the $V_{zz}$ direction. Therefore we fixed $\eta \approx 0$. For $T < T_N$ the spectra were fitted with a general Hamiltonian of the form

$$\boldsymbol{H} = -g\,\mu_N H_{hf}(\theta, \Phi) + \frac{eQV_{zz}}{4I(I+1)} \cdot \left\{3I_z^2 - I^2 + \frac{\eta}{2}(I_+^2 - I_-^2)\right\}, \tag{9}$$

where $\theta$ and $\Phi$ are the angles of $H_{hf}$ with respect to the EFG principal axis system.

The fits were insensitive to $\Phi$ due to the vanishing value of the asymmetry parameter. Analysis of the 4.2 K spectra showed that the main axes of the nearly axial symmetric EFG tensors are tilted by an angle of about $\theta \simeq 26°$ and 22° with respect to the hyperfine field directions. Assuming for $Li_2Mn_{0.98}Fe_{0.02}F_5$ and $Na_2Mn_{0.98}Fe_{0.02}F_5$ an orientation of $V_{zz}$ parallel to the bridging (Mn, Fe)-F bonds, i.e. a mean angle of 29.3° and 23.8° with respect to the $b$ axis [19], we estimated the magnetic hyperfine field directions at mean angles of about 3(3)° and 2(3)° with the $b$ axes, respectively. This means that the analysis above is not sensitive enough to extract small canting angles $\varphi$ as calculated from (8). The moments in $Li_2Mn_{0.98}Fe_{0.02}F_5$ and $Na_2Mn_{0.98}Fe_{0.02}F_5$ lie nearly along the chain directions.

The isomer shifts IS = 0.422(8) mm/s and IS = 0.436(8) mm/s (relative against Fe metal) at 4.2 K in $Li_2Mn_{0.98}Fe_{0.02}F_5$ and $Na_2Mn_{0.98}Fe_{0.02}F_5$, respectively, are characteristic for $Fe^{3+}$ and were also observed in analogous chain structures. The observed quadrupole splittings are $\Delta E^Q = 1/2\, e^2 Q V_{zz}(1+\eta^2/3)^{1/2}$ = 0.977(8) mm/s and 0.975(8) mm/s. These values are large for a $^6S$ state. This might be due to the isolated chain structure and the different bond conditions, as already discussed in [13]. The positive values of the quadrupole splittings show that the octahedra are distorted in such a way that the four equatorial fluorine anions are closer to the iron ion and the two axial anions are more remote, in agreement with the interatomic distances listed in Table 1 and X-ray study on single crystals of $(NH_4)_2Mn_{0.98}Fe_{0.02}F_5$ [29].

Three-dimensional magnetic ordering in $Li_2Mn_{0.98}Fe_{0.02}F_5$ and $Na_2Mn_{0.98}Fe_{0.02}F_5$ is apparent in the low-temperature magnetically split spectra. Above $T_N$ we observe an unusual (non-Brillouin) behaviour in the temperature dependence of the internal fields. As observed in the chain compounds $Rb_2Mn_{0.99}Fe_{0.01}F_5(H_2O)$ and $(NH_4)_2Mn_{0.98}Fe_{0.02}F_5$ with strong anisotropy [13, 17], the transition from the paramagnetic state to the magnetically ordered state is accompanied by slow and fast relaxation phenomena below and above $T_N$, respectively, which may be attributed to non-linear excitations of domain walls. This effect masks the transition usually observed near the critical point and prohibits an accurate determination of the ordering temperature by Mössbauer spectroscopy. The possible occurrence of slow spin-spin relaxation may be excluded as explained in [13]. Additionally, we have considered the occurrence of superparamagnetic effects or spin glass behaviour. However, as the magnetically split spectra are still observed above the ordering temperature, this would create a great discrepancy with other experimental results [13]. The origin of the broadened asymmetric spectra in the region near the critical point must be attributed to residual 1-d correlations above the phase transition [11].

The detailed theoretical analysis of domain wall dynamics and solitons in magnetic chains shows [35] that, in a certain range above the critical temperature, the density of $\pi$ domain walls and their motion determines the spin autocorrelation function $\langle \boldsymbol{S}(0)\boldsymbol{S}(t)\rangle$, which is obtained by measuring the fluctuating hyperfine field $\boldsymbol{H}_{hf}(t) \propto \boldsymbol{S}(t)$ (see (5)).

Finally, the Mössbauer spectra of $Li_2Mn_{0.98}Fe_{0.02}F_5$ and $Na_2Mn_{0.98}Fe_{0.02}F_5$ were successfully fitted by

adopting the Blume and Tjon relaxation model [36, 37], in which it is assumed that the hyperfine field jumps stochastically between the two possible values $+H_{hf}$ and $-H_{hf}$. This takes into account a time-dependent Hamiltonian. Thus, the hf interaction is replaced by a fluctuating effective field, and the decrease in the fluctuation rate causes line broadening, asymmetric spectra, and related phenomena. The relaxation phenomena are closely related to the excess linewidths of the transmission lines in the Mössbauer spectrum. Consequently these have to be determined with optimal accuracy. Therefore one would like to have small residual linewidths, linear backgrounds and good $S/N$ ratio, and everything with in a reasonable measuring time. These causes conflict. In our experiments we have studied a sample with 0.12 mg $^{57}$Fe (or 6 mg natural Fe) per cm$^2$ absorber surface. The corresponding residual linewidths at low- and high-temperatures of 0.27 mm/s are acceptable. The excess linewidth with respect to the natural linewidth of 0.194 mm/s is always observed and is independent of the relaxation process in the chain.

In applying the Blume-Tjon model, our Mössbauer spectra can be fully fitted at all temperatures, with the flipping rate $G_\omega$ and the ratio of probabilities that $H_{hf}$ jumps to $-H_{hf}$ and vice versa, as the only adjustable, temperature dependent parameters. In these fits the other Mössbauer parameters were kept at the values determined at low temperatures, see Table 3. From the resolved spectra, clusters with different relaxation frequencies must be present in the temperature range near 13 K. Between 9 and 13.5 K, there appears in addition – as mentioned above – a central asymmetric doublet due to faster relaxation that is still observable up to 30 K (see Figures 5 and 6).

As may be seen from the figures (note the different velocity scales in the figures), the fits reproduce the observed spectra remarkably well. The resulting values for $G_\omega$ are plotted in Fig. 7 on a logarithmic scale versus the inverse temperature.

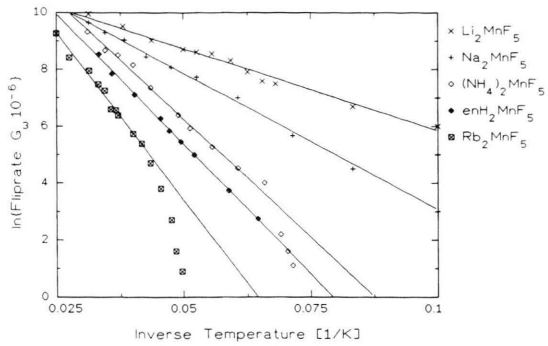


Fig. 7. Comparison of the spin-flip rates for $Li_2Mn_{0.98}Fe_{0.02}F_5$ and $Na_2Mn_{0.98}Fe_{0.02}F_5$ with the spin-flip rates for previous studies of $(NH_4)_2Mn_{0.98}Fe_{0.02}F_5$ [17], $enH_2Mn_{0.98}Fe_{0.02}F_5$ [30], and $Rb_2Mn_{0.99}Fe_{0.01}F_5(H_2O)$ [13]. The straight lines $\ln(G_\omega) \propto -E_A/T$ show the exponential dependence of $G_\omega$ on the reciprocal temperature $1/T$.

Knowing that the solitons are moving above $T_N$, one would like to investigate what the soliton dynamics looks like. Therefore it is of interest to compare the experimental data with the predictions from the soliton theory. In Fig. 7 we compare the spin-flip rates for $Li_2Mn_{0.98}Fe_{0.02}F_5$ and $Na_2Mn_{0.98}Fe_{0.02}F_5$ with the spin-flip rates for $(NH_4)_2Mn_{0.98}Fe_{0.02}F_5$ [17], $enH_2Mn_{0.98}Fe_{0.02}F_5$ [30], and $Rb_2Mn_{0.99}Fe_{0.01}F_5(H_2O)$ [13, 14]. The straight lines $\ln(G_\omega) \propto -E_A/T$ show the exponential dependence of $G_\omega$ on the reciprocal temperature $1/T$ with the parameters $E_A/k = 55(5)$ K for $Li_2Mn_{0.98}Fe_{0.02}F_5$, $E_A/k = 95(5)$ K for $Na_2Mn_{0.98}Fe_{0.02}F_5$, $E_A/k = 161(5)$ K for $(NH_4)_2Mn_{0.98}Fe_{0.02}F_5$, $E_A/k = 184(5)$ K for $enH_2Mn_{0.98}Fe_{0.02}F_5$ and $E_A/k = 234(5)$ K for $Rb_2Mn_{0.99}Fe_{0.01}F_5(H_2O)$, which are characteristic for an activated soliton process [38]. The temperatures at which the drop of the flip rates $\ln G_\omega$ occur in Fig. 7 correspond to 8 K, 11 K, 14.5 K and 26.5 K [13, 17]. One may interpret this as a blocking of the domain motion by the onset of 3-d long-range order. The 3-d

Table 3. Values at 4.2 K of the magnetic hyperfine field $H_{hf}$, quadrupole splitting $\Delta E^Q$, quadrupole shift $2\varepsilon$, and $\theta(V_{zz}, H_{hf})$. The angle $\vartheta$ means $\vartheta = (180° - \beta(\text{Mn-F-Mn}))/2$, see Table 1.

| Compound | $H_{hf}$ [kOe] | $\Delta E^Q$ [mm/s] | $2\varepsilon$ [mm/s] | $\theta$ [°] | $\vartheta$ [°] |
|---|---|---|---|---|---|
| $Li_2Mn_{0.98}Fe_{0.02}F_5$ | 546(3) | 0.977(5) | 0.635(8) | 26(3) | 29.3 |
| $Na_2Mn_{0.98}Fe_{0.02}F_5$ | 545(3) | 0.975(8) | 0.814(8) | 22(3) | 23.8 |
| $(NH_4)_2Mn_{0.98}Fe_{0.02}F_5$ | 525(3) | 0.720(8) | 0.628(8) | 17(3) | 18.3 |
| $Rb_2Mn_{0.99}Fe_{0.01}F_5(H_2O)$ | 521(3) | 0.840(8) | 0.838(8) | 2(3) | 2.3 |

Table 4. Values of bridge angle, activation energy $E_A$ from Mössbauer experiment, 1-d exchange energy $J$, ratio $J/D$, and width of domain wall $N_d$, for the compounds listed.

| | $\beta$(Mn-F-Mn)[°] | $E_A/k$[K] | $J/k$[K] | $\lvert J/D \rvert$ | $N_d$[A] |
|---|---|---|---|---|---|
| $Li_2Mn_{0.98}Fe_{0.02}F_5$ | 121.5 | 55(5) | −5.9 | 1.6 | 4.7 t.w. |
| $Na_2Mn_{0.98}Fe_{0.02}F_5$ | 132.5 | 95(5) | −8.5 | 2.4 | 5.9 t.w. |
| $(NH_4)_2Mn_{0.98}Fe_{0.02}F_5$ | 143.4 | 161(5) | −10.6 | 3.0 | 6.9 [17] |
| $enH_2Mn_{0.98}Fe_{0.02}F_5$ | 159.5 | 184(5) | −13.6 | 3.6 | 8.0 [30] |
| $Rb_2Mn_{0.99}Fe_{0.01}F_5(H_2O)$ | 175.4 | 234(5) | −20.8 | 5.9 | 10.1 [13] |

Table 5. Comparison between the derived anisotropy constants $D$ on the basis of the sine-Gordon equation (SG) and classical domain wall theory (CS). $E_A$ and $E_s$ (see (3) and (4)) are the Mössbauer activation and soliton creation energy, respectively.

| | Anisotropy constant $D/k$ [K] | | |
|---|---|---|---|
| Model | SG | CS | |
| | 14.6 | 5.9 | $E_A = E_s$ |
| | 3.7 | 1.5 | $E_A = 2E_s$ |

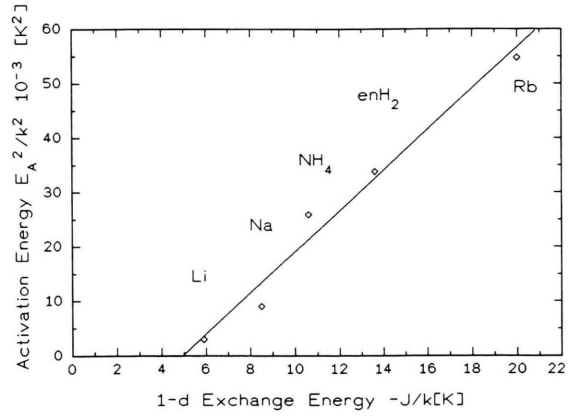


Fig. 8. Calculation of the anisotropy constant $D/k$ from the dependence of $E_A^2$ on the intrachain exchange interaction $J/k$. Inserting $E_A = 2E_s$ we derived $D/k = 3.7(2)$ K in agreement with magnetic susceptibility measurements on single crystal [17, 29, 30].

ordering points are few degrees lower. We determined the values of the Néel temperature $T_N = 4.2(5)$, $T_N = 6.0(5)$, $T_N = 8.5(5)$ K [17], and $T_N = 23(1)$ K [13] from susceptibility measurements, respectively.

The trend of the activation energy from Mössbauer experiments is quite convincing. Since our main interest was to determine the anisotropy energy from Mössbauer experiments – as described above – we consider that such a decrease of activation energy $E_A$ with decreasing exchange energy $J/k$ may be understood from the domain wall theories of (3) and (4).

As mentioned in [13] this approximation may be convenient if the spin value is large, so that the classical spin vector is approached, and if the characteristic wavelengths of the fluctuations in the spin system (e.g. the widths of the solitons $N_s$) are large compared to the lattice spacing.

Assuming that the domain wall theories are also valid in the present case of a random system, and inserting in (3) and (4) the experimental values of $J/k$, $E_A = E_s$ or $E_A = 2E_s$, and the average spin of the solid solutions $S \simeq 2$, we can now estimate from the dependence of $E_A^2$ as a function of the intrachain exchange interaction $J$ the anisotropy constant $D$ (see Fig. 8), which may be compared with the predictions from soliton theories (see Table 5). It is noteworthy that experimental methods like spin cluster excitations [39] and inelastic neutron scattering [40, 41], probe the excitation spectrum and find excitation energies roughly equal to $2E_s$. Considering that the single-ion anisotropy of Fe(III) in the Mn(III) matrix amounts to $\lvert D/k \rvert \simeq 3.5$ K we conclude from the $D$ values in Table 5 that the dominating relaxation mechanism also observed in the Mössbauer spectra is the thermal excitation of soliton pairs. The single-ion anisotropy $D/k = 3.7$ K derived from solutions of the sine-Gordon approximation of (4) is in fair agreement with the $D$ values derived from magnetic susceptibility measurements on single crystals of the solid solutions $(MH_4)_2Mn_{1-x}Fe_xF_5$ with $x = 0$ [17, 25] and $x = 0.02$ [17] and $Rb_2MnF_5(H_2O)$ [13] (see Table 2).

Single soliton excitations are only found in calculations of finite chains if free ends are considered [42]. Moreover, for a chain with $N$ spins, the statistical weight for exciting single solitons and soliton pairs will be proportional to $N$ and $N^2$, respectively. Therefore, experimentally, single soliton excitations can be

neglected for sufficiently long chains. In our Mössbauer experiments on $Li_2MnF_5$ and $Na_2MnF_5$, two distinct subspectra are observed up to temperatures of 13 K and 14 K, respectively, where the intensity of one subspectra becomes negligible. The first one is the slowly relaxing subspectrum, which shows an activation energy of $E_A = 2E_s$. The second subspectrum, the doublet, relaxes fast with a temperature independent relaxation rate of $10^9\ s^{-1}$. De Jongh and his group identified this subspectrum with the intra-band excitations [35] since the level splittings in the soliton pair band are small with respect to the temperature, resulting in a fast paramagnetic relaxation behaviour. It is worth mentioning that these rapid fluctuations must be restricted to only parts of the chain. Otherwise the slowly relaxing component would not be present.

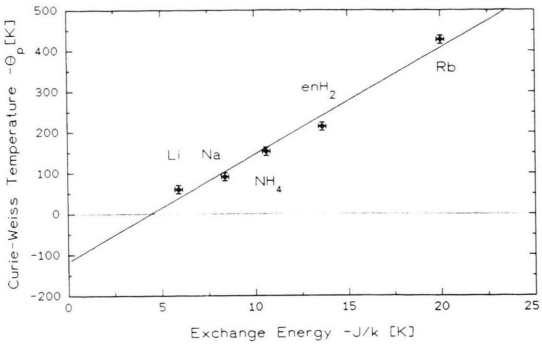


Fig. 9. Dependence of the Curie-Weiss temperature $\theta_p$ on the 1-d exchange energy $J/k$. The straight line represents the linear least-squares fit and is a guide to the eye.

## Conclusion

It is worthwhile to establish that the dependence of the activation energy $E_A^2$ as a function of the 1-d exchange energy $J$ calculated by a least squares fit yields an intercept on the $J$ axis of about $-5$ K (see Figure 8). In the light of our results we have to conclude that the exchange energies derived from the sine-Gordon equation (4) are different from the exchange energies determined from the susceptibility measurements of (7). It is well-known that the Fisher model, (7), applied on susceptibility measurements favours within the 1-d magnetic phase the antiferromagnetic exchange energy, whereas the local method of Mössbauer spectroscopy may support the effective exchange energy, possibly two contributions of an antiferromagnetic and a ferromagnetic part.

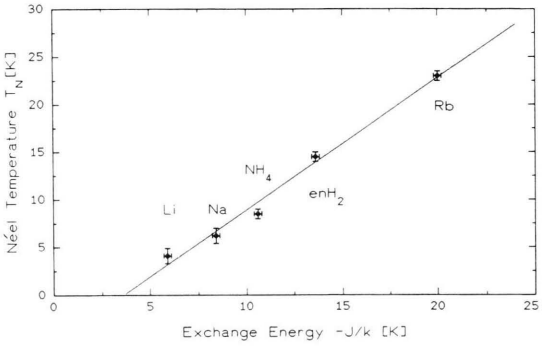


Fig. 10. Dependence of the derived Néel temperatures on the 1-d exchange energy.

The suggestion that a ferromagnetic superexchange contribution favored for 90° cation-anion-cation interaction reduces the antiferromagnetic coupling between the manganese ions, at least in the range of very low bridge angles, is confirmed by the dependence of the Curie-Weiss temperatures $\theta_p$ and Néel temperatures $T_N$ vs. the 1-d exchange energies $J$ in Fig. 9 and Fig. 10, respectively. In accordance with the rules of Anderson [43], Goodenough [44], and Kanamori [45], the superexchange interaction can be qualitatively determined from the symmetry relation of the atomic orbitals involved [19, 46]. The electronic configuration of a $Mn^{III}$ ion in its high-spin state is $d\varepsilon^3 d_{z^2}^1$. The Jahn-Teller distortion along the chain axis indicates that the half-occupied $d_{z^2}^2$ orbitals are all pointing in

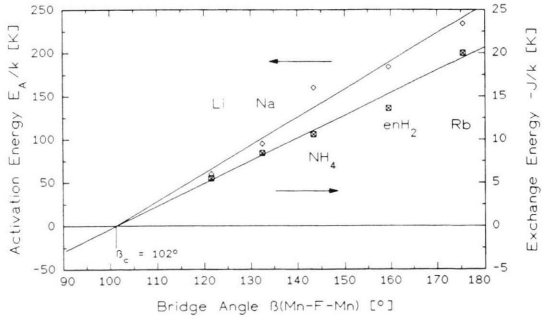


Fig. 11. Linear extrapolations of the experimental data of activation and exchange energies on the Mn-F-Mn bridge angle $\beta$. The angle for which superexchange $J$ vanishes is $\beta_c \simeq 102°$. Note that, if the 180° path the $Mn^{3+}$-F-$Mn^{3+}$ interaction $J < 0$ is antiferromagnetic, the 90° path superexchange should be ferromagnetic $J > 0$.

this direction. If Mn-F-Mn is linear, $\sigma$ bonds are formed by the $p_z$ orbital of fluorine and the $d_z^2$ orbital of manganese (iron). Since the orbitals are nonorthogonal, antiferromagnetic coupling results between these metal ions. As shown in [19, 46], the antiferromagnetic interactions decrease with a reduction in the Mn-F-Mn bridge angle. This is due to a decrease in the overlap of the $d_z^2$ and $p_z$ orbitals involved. The simple linear extrapolation of the activation energy $E_A$ and 1-d exchange energy in Fig. 11 seems to support this model. A more detailed study is now under consideration. Attempts for a quantification of the Goodenough-Kanamori rules for the exchange interactions and their angular dependence by the Angular Overlap Model and Extended Hückel calculations have been performed by Atanasov [47, 48].

*Acknowledgements*

We thank M. Atanasov and W. Massa for many helpful discussions. Support of this work by the Bundesminister für Forschung und Technologie and the Fonds der Chem. Industrie is gratefully acknowledged.

[1] J. P. Boucher, Hyperfine Interactions **49,** 423 (1989).
[2] J. Villain, Physica **79 B,** 1 (1975).
[3] K. Maki, Phys. Rev. **214,** 335 (1981).
[4] R. J. Mileska, J. Appl. Phys. **52,** 1950 (1981).
[5] M. Steiner, J. Villain, and C. G. Windsor, Adv. Phys. **25,** 87 (1976).
[6] M. Steiner, Ordering in Strongly Fluctuating Condensed Matter Systems, ed. by T. Riste, Plenum Publishing Corporation, 1980.
[7] J. K. Kjems and M. Steiner, Phys. Rev. Lett. **41,** 1137 (1978).
[8] L. J. de Jongh, Magneto-Structural Correlations in Exchange Coupled Systems, NATO ASI Series, D. Seidel Publishing Company, 1983.
[9] H. J. Mikeska and M. Steiner, Adv. Phys. **40,** 191 (1991).
[10] C. Kittel and J. K. Galt, Sol. State Phys. **3,** 437 (1956).
[11] H. J. M. de Groot, Thesis, Leiden, The Netherlands 1986.
[12] L. J. de Jongh, J. Appl. Phys. **53,** 8018 (1982).
[13] J. Pebler, Inorg. Chem. **28,** 1038 (1989).
[14] J. Pebler, Hyperfine Interactions **45,** 363 (1989).
[15] J. Pebler and D. Babel, Organic and Inorganic Low-Dimensional Crystalline Materials, NATO ASI Series, Plenum Press, 1987.
[16] J. Pebler, Hyperfine Interactions **49,** 490 (1989).
[17] C. Frommen and J. Pebler, Hyperfine Interactions **96,** 51 (1995).
[18] W. Massa, M. Molinier, and J. Pebler, J. Fluorine Chem. **72,** 171 (1995).
[19] J. Pebler, W. Massa, H. Lass, and B. Ziegler, J. Sol. State Chem. **71,** 87 (1987).
[20] W. Massa, Acta Crystallogr. Sect. C **42,** 644 (1986).
[21] from Quantum Design, San Diego, USA.
[22] D. R. Sears and J. L. Hoard, J. Chem. Phys. **50,** 1066 (1969).
[23] P. Bukovec and V. Kaucic, Acta Crystallogr. Sect. B **34,** 3339 (1978).
[24] J. M. Dance, private communication.
[25] J. Kida and T. Watanabe, J. Phys. Soc. Japan **34,** 952 (1973).
[26] M. Mangold, Diplomarbeit, Marburg 1994.
[27] M. E. Fisher, Am. J. Phys. **32,** 343 (1964).
[28] T. Smith and S. A. Friedberg, Phys. Rev. **176,** 660 (1968).
[29] C. Frommen, Thesis, Marburg, Germany 1994.
[30] C. Frommen, L. Schröder, U. Bentrup, W. Massa, and J. Pebler, Z. Naturforsch. **50 b,** 1627 (1995).
[31] O. Kampe, C. Frommen, and J. Pebler, Z. Naturforsch. **48 b,** 1112 (1993).
[32] M. Molinier, C. Frommen, W. Massa, T. Roisnel, and J. Pebler, Z. Naturforsch. **48 a,** 1054 (1993).
[33] J. L. Soubeyrous, private communications.
[34] M. Winkelmann, private communications.
[35] H. H. A. Smit, Thesis, Leiden, The Netherlands, 1988.
[36] M. Blume and J. A. Tjon, Phys. Rev. **B 165,** 446 (1968) and **B 174,** 351 (1968).
[37] J. Pebler, J. Phys. Status Solid **A 78,** 589 (1983).
[38] R. C. Thiel, H. de Graaf, and L. J. de Jongh, Phys. Rev. Lett. **47,** 1415 (1981).
[39] Q. A. P. van Vlimmern, C. H. W. Swüste, W. J. M. van der Steeg, J. H. M. Stoelinga, and P. Wyder, Phys. Rev. **B 21,** 3005 (1980).
[40] S. E. Nagler, W. J. L. Buyers, R. L. Armstrong, and B. Briat, Phys. Rev. **B 28,** 3873 (1983).
[41] W. J. L. Buyers, M. J. Hogan, R. L. Armstrong, and B. Briat, Phys. Rev. **B 33,** 1727 (1986).
[42] J. D. Johnson and J. C. Bonner, Phys. Rev. **B 22,** 251 (1980).
[43] P. W. Anderson, Phys. Rev. **79,** 350 (1950).
[44] J. B. Goodenough, Magnetism and Chemical Bond, New York 1963.
[45] J. Kanamori, J. Phys. Chem. Solids **10,** 87 (1959).
[46] W. Massa, M. Molinier, and J. Pebler, J. Fluorine Chem. **72,** 171 (1995).
[47] M. Atanasov, private communication.
[48] M. Atanasov and S. Angelov, Chem. Physics **150,** 383 (1991).